Liquid Crystals
Publication details, including instructions for authors and subscription information:
http://www.informaworld.com/smpp/title~content=t713926090

Synthesis and characterization of new azomethine derivatives exhibiting liquid crystalline properties

Luminita Marin[a]; Silvia Destri[b]; William Porzio[b]; Fabio Bertini[b]
[a] 'P. Poni' Institute of Macromolecular Chemistry, 41A Grigore Ghica Voda Alley, 700487 Iasi, Romania
[b] Istituto per lo Studio delle Macromolecole del C.N.R., via E. Bassini 15, 20133 Milano, Italy

To cite this Article Marin, Luminita , Destri, Silvia , Porzio, William and Bertini, Fabio(2009) 'Synthesis and characterization of new azomethine derivatives exhibiting liquid crystalline properties', Liquid Crystals, 36: 1, 21 — 32
To link to this Article: DOI: 10.1080/02678290802638423
URL: http://dx.doi.org/10.1080/02678290802638423

Liquid Crystals,
Vol. 36, No. 1, January 2009, 21–32

Taylor & Francis
Taylor & Francis Group

Synthesis and characterization of new azomethine derivatives exhibiting liquid crystalline properties

Luminita Marin[a]*, Silvia Destri[b], William Porzio[b] and Fabio Bertini[b]

[a]*'P. Poni' Institute of Macromolecular Chemistry, 41A Grigore Ghica Voda Alley, 700487 Iasi, Romania;* [b]*Istituto per lo Studio delle Macromolecole del C.N.R., via E. Bassini 15, 20133 Milano, Italy*

(Received 1 October 2008; final form 20 November 2008)

Azomethine liquid crystals (LCs), constituted by symmetric and asymmetric bithiophene or fluorene units as chromophores, were designed and synthesised. Their thermotropic behaviour was investigated using optical microscopy, differential scanning calorimetry, and wide angle X-ray diffraction. A lowering of transition temperatures was obtained by the introduction of the lateral methyl group as compared with unsubstituted compounds. The observed LC phases possess the classical textures of calamitic LCs. The optical properties of the target compounds were evaluated, both in solution and in solid state. A blue fluorescence was observed for fluorene containing compounds and a green fluorescence was observed for analogous bithiophene containing compounds. The introduction of a methyl lateral group onto the aromatic rings led to a remarkable increase in the solution emission properties.

Keywords: azomethine; thiophene; fluorene; liquid crystals; optical properties

1. Introduction

Thermotropic liquid crystals (LCs) have assumed great technological importance during recent years. The design of novel thermotropic LCs as advanced functional materials involves the suitable selection of a core fragment, linking group, and terminal functionality. LC compounds containing heterocyclic rings have acquired large interest due to their wide range of potential applications, namely in the optoelectronic, electrical, and biomedical fields (*1–3*). LCs containing heterocyclic cores, such as thiophene, are of particular interest due to their slightly bent structure, which leads to features including a reduced packing ability (generally giving rise to lower melting points than their phenyl counterparts), a medium to strong lateral dipole, high anisotropy of the polarisability, and low viscosity (*4*). Extensive studies have shown that thiophene and fluorene materials exhibit a variety of interesting optical, electrical, and photoelectric properties in the solid state (*5, 6*). These compounds have been proposed as potential candidates for the active layer in organic-based optoelectronic devices such as light-emitting diodes (LEDs), photovoltaic cells (PVCs), field-effect transistors (FETs), and light-emitting field-effect transistors (LETs) (*7–9*). A large number of Schiff base compounds have been synthesised because they exhibit nematic and smectic mesophases (*10*). The interest in the synthesis and structural investigations of LCs containing Schiff bases in their mesogenic units has considerably increased due to their potential applications in non-linear optics and the optical storage field. Their thermal and environmental stabilities are also important features for these applications, where upon laser beams, local overheating and material damage are commonly observed (*11, 12*).

The use of LC molecules is justified by the versatility of the targets achievable, according to the applications, due to the dimensionality reduction, i.e. less efficient packing with respect to 3D single crystals, or the increase of mesophase crystallite size, namely favouring the proper orientation with respect to polycrystalline materials.

In this context, our interest has been focused on low molecular mass organic compounds containing two bithiophene or fluorene units directly linked by a benzylidene–aniline unit.

In this paper, we report on the synthesis, mesomorphic behaviour, and the electrical and photophysical properties of the azomethine derivatives shown in Scheme 1. To enlarge the overall conjugation length, all the compounds were designed with two aromatic arms around the central azomethine bond, promoting backbone polarisation.

The rationale design for these new structures is as follows:

- thiophene rings were chosen because oligothiophene- and thiophene-based polymers exhibit remarkable charge carrier mobilities (*5*);
- the fluorene units show high fluorescent efficiency and appreciable stability due to their rigid

*Corresponding author. Email: lmarin@icmpp.ro

ISSN 0267-8292 print/ISSN 1366-5855 online

DOI: 10.1080/02678290802638423
http://www.informaworld.com

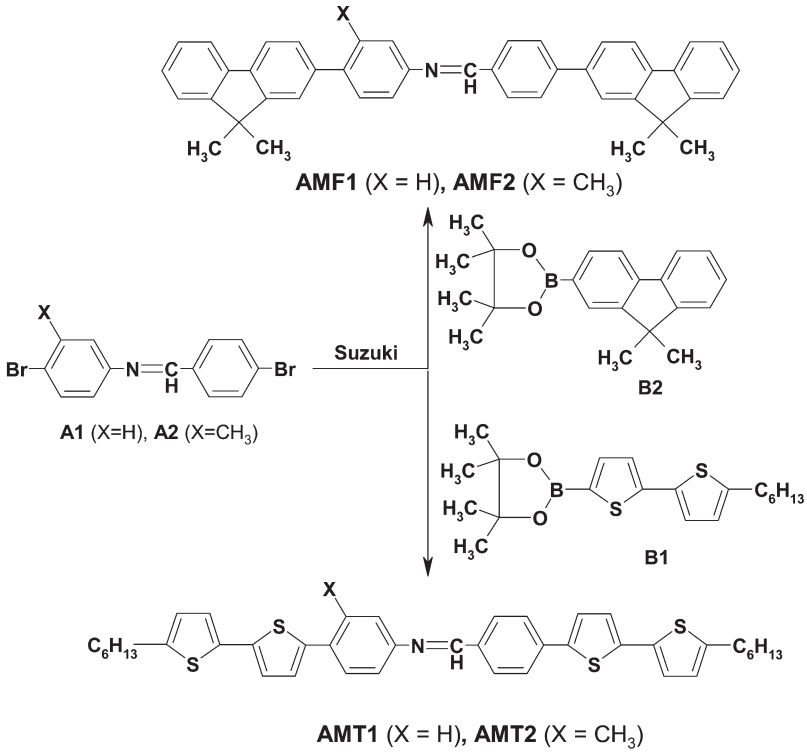

Scheme 1. Synthesis of the azomethine derivatives AMF and AMT. Suzuki coupling conditions: THF, 70°C, K_2CO_3 (2M), $(PPh_3)_4Pd$.

structure and low highest occupied molecular orbital (HOMO) level (*13*);
- the aromatic azomethine unit was selected because the compounds containing imine linkages exhibit semiconducting properties, thermal stability, thermotropic potential, and the ability to form organometallic complexes (*14*);
- the terminal hexyl chains and the lateral methyl group improve solubility, hence processability, and decrease phase-transition temperatures (*1*).

2. Results and discussions

2.1. Synthesis

The synthetic route to prepare the LC materials was carried out according to Scheme 1. The azomethine-based aryl bromides (**A1**, **A2**) were prepared from 4-bromo-benzaldehyde and 4-bromo-aniline or 4-bromo-3-methylaniline respectively, using an acid-catalysed condensation reaction (*15*). The boronic derivative of fluorene was synthesised by methylation in the 9-position of the starting material followed by the coupling with 2-isopropoxy-(4,4,5,5-tetramethyl)1,3,2-dioxoborolane through lithium fluorene derivative formation in the 2-position. The final step (see Scheme 1) was the Suzuki coupling between azomethine aryl bromides **A1** and **A2** and fluorene boronic derivative **B2** to afford compounds **AMF1** and **AMF2**, while the reaction of the bromoderivatives with the corresponding bithiophene borolane yielded **AMT1** and **AMT2**, respectively. Elemental analysis (C, H, N) was in excellent agreement with the calculated values for all new compounds. ^{1}H nuclear magnetic resonance (NMR) and Fourier transform infrared (FTIR) spectroscopic analyses further confirmed the molecular structures.

2.2. Mesophases and thermal properties

The transition temperatures and the thermal stability of the compounds have been investigated by polarising optical microscopy (POM), differential scanning calorimetry (DSC), and thermogravimetric analysis (TGA) – the results are collected in Table 1.

As small amounts of the material thermally decomposed, drastically affecting the thermotropic behaviour of the LCs, we evaluated the thermal stability by TGA, considering the onset of thermal decomposition, i.e. the temperature corresponding to an initial 1% of weight loss ($T_{1\%}$). The TGA traces presented in Figure 1(a) show that the azomethine derivatives are thermally stable in an inert atmosphere up to 300–366°C. At higher temperatures all the investigated compounds show a very fast weight loss. The derivative thermogravimetry (DTG) curves provide evidence that the degradation process takes place

Table 1. Thermal behaviour of the compounds **AMF1**, **AMF2**, **AMT1** and **AMT2**.

Code	DSC Transition temperature in °C (enthalpy changes in J g^{-1})[a, b]	POM Transition temperature in °C[a]	$T_{1\%}$[d] (°C)	T_{max}[e] (°C)
AMF1	1H: Cr 323 (104.1) N 350 (1.5) I	1H: Cr 320 N 370 I[b]		
	C: I 336 (2.6) N 271 (101.4) Cr	C: I 365 N 275 Cr	300	446
	2H: Cr 323 (103.5) N 353 (2.1) I	2H: Cr 325 N 370 I		
AMF2	1H: Cr 230 (51.1) N 282 (0.8) I	1H: Cr 242 N 286 I[b]		
	C: I 269 (1.7) N 133 (13.5) Cr	C: I 283 N 195 Cr	299	445
	2H: Cr 232 (55.1) N 292 (1.3) I	2H: 220 N 287 I		
AMT1	1H: Cr 130 (28.7) Sm 254 (18.8) N 360 (2.0) I	1H: Cr 130 Sm 242 N 366 I[c]		
	C: I 323(2.1) N 220 (17.5) Sm 71 (8.5) Cr	C: I 361 N 195 Sm 79 Cr	366	437
	2H: Cr 112 (11.3) Sm 245 (17.1) N 348 (1.4) I			
AMT2	1H: Cr 128 (59.2) Sm 230(1.1) N 316 (3.0) I	1H: Cr 136 Sm 243 N 326 I[c]		
	C: I 294 (3.0) N 207 (0.6) Sm 79 (35.3) Cr	C: I 309 N 192 Sm 81.3 Cr	347	438
	2H: Cr 116 (39.3) Sm 227 (0.7) N 313 (3.0) I			

[a]1H=first heating scan, C=cooling scan; 2H=second heating scan; Cr=crystalline, Sm=smectic mesophase, N=nematic mesophase, I=isotropic. [b]Determined at heating and cooling rates of 90°C min^{-1}. [c]Determined at heating and cooling rates of 10°C min^{-1}. [d]The initial decomposition temperature at 1% weight loss determined by TGA. [e]The temperature at maximum rate of weight loss measured by TGA.

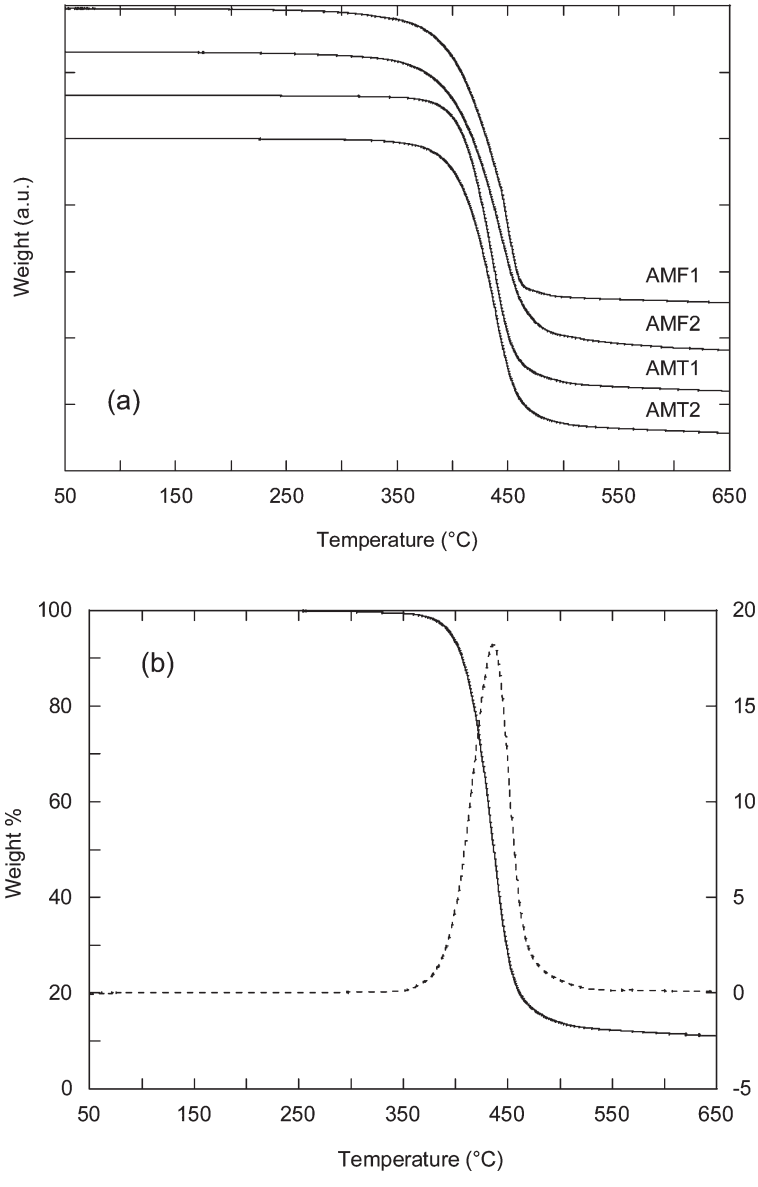

Figure 1. (a) TGA traces of azomethine derivatives. (b) TGA (solid line) and DTG (dashed line) thermograms of AMT1.

in a single step; as an example, the DTG curve of **AMT1** is reported in Figure 1(b). The T_{max} values, i.e. the temperature corresponding to the maximum rate of weight loss, range between 437 and 446°C and the bithiophene containing compounds approach the lower limit of the T_{max} range. As presented in Table 1, the characteristic $T_{1\%}$ values for **AMT** compounds are considerably higher than those of the **AMF** samples, with an increase of more than 50°C. This depends on the different thermal robustness of the aromatic units.

By comparing the TGA curves of the compounds containing the methyl group to those of the unsubstituted ones, it turns out that the presence of the methyl lateral group has a smaller effect than the influence exerted by the nature of the aromatic units. In fact, **AMT1** shows a significant increase in the $T_{1\%}$ value (ca. 20°C) as compared to **AMT2**, probably due to the closer packing in the crystalline structure.

The degradation process ends at around 500°C for all the azomethine compounds and no more weight loss is observed thereafter, for the experiments carried out in inert atmosphere. The maximum residue yield calculated at 650°C is noticed for **AMF1** (around 1 wt.%), whereas the other compounds show similar residues (ca. 11 wt.%).

Conversely, POM measurements indicate that **AMT1** and **AMT2** are less stable than **AMF1** and **AMF2**, i.e. in air the thiophene rings decompose at lower temperatures than fluorene units.

The fluorene containing compounds (**AMF1** and **AMF2**) display similar thermotropic behaviour, the main difference being the lower transition temperatures for **AMF2** due to the presence of the methyl lateral groups. As shown in Figure 2(a), the compounds **AMF1** and **AMF2** exhibit a marbled texture with inversion walls, possibly with tilt character – these are unstable and disappear when the temperature increases. Before isotropisation, a Schlieren texture containing two- and four-brush declinations appears for a short time, excluding the possibility of biaxiality in these phases (Figure 2(b)) (*16, 17*).

When the isotropic liquid is cooled, the nematic state appears at the clearing point in the form of round droplets that grow leading to the marbled texture (Figures 3(a) and (b)). Upon further cooling, the nematic state crystallises. On the basis of these observations, we assumed that **AMF1** and **AMF2** compounds form an enantiotropic nematic mesophase.

The compounds containing bithiophene units also present similar thermotropic behaviour. They have poor thermal stability in air; the superposing of thermal degradation was visible under polarised light in the first heating scan carried out at 10°C min^{-1}. In order to avoid such a decomposition, the **AMT**

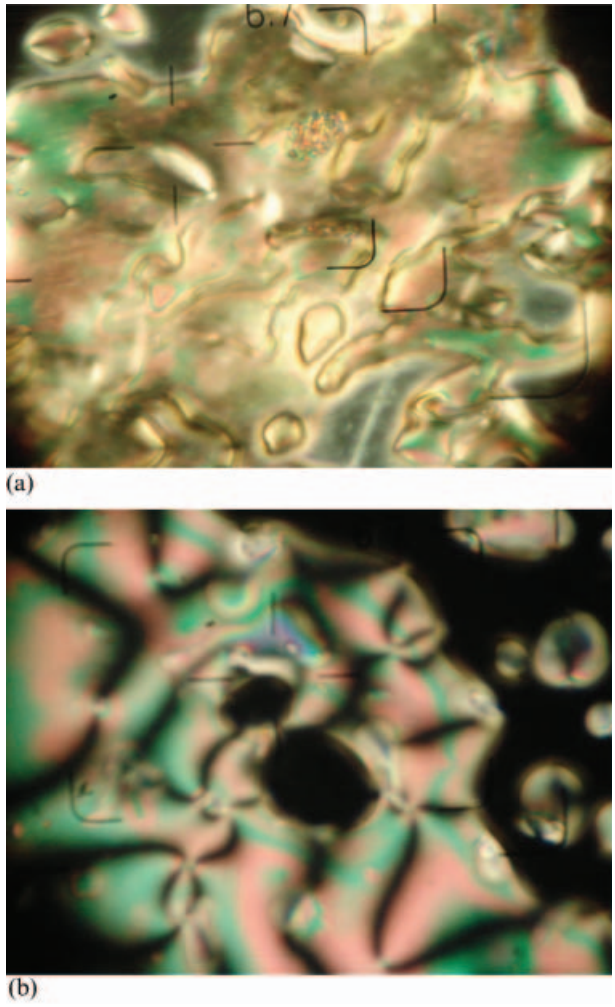

Figure 2. Photomicrographs of (a) the nematic texture with surface inversion lines at 325°C, second heating and (b) the nematic Schlieren texture at 365°C, first heating for compound AMF1 (40 x).

samples were heated and cooled using a temperature rate of 90°C min^{-1}, yielding two evident kinds of texture. In the first heating scan, the samples melt into a birefringent viscous fluid with a fine grain texture that turns into a marbled texture with high fluidity. Such a texture is evident in the cooling scan, i.e. nematic droplets, which are transformed into a marbled texture, appear from the isotropic fluid (Figure 4(a)). Upon further cooling, the marbled texture changes into a striated texture, ascribed by some authors to the smectic C mesophase (Figure 4(b)) (*16, 18, 19*), which finally freezes. The **AMT2** compound has lower transition temperatures than the **AMT1**, due to the presence of the bulky methyl group.

DSC measurements confirm the phase transitions observed by the POM investigations. These two methods indicate similar transition temperatures,

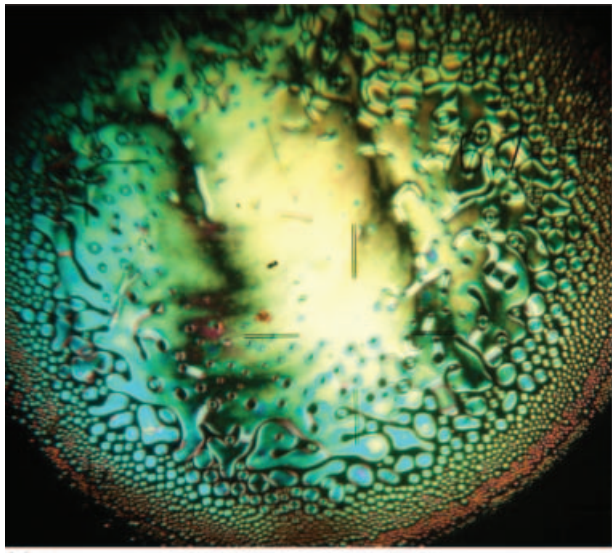

(a)

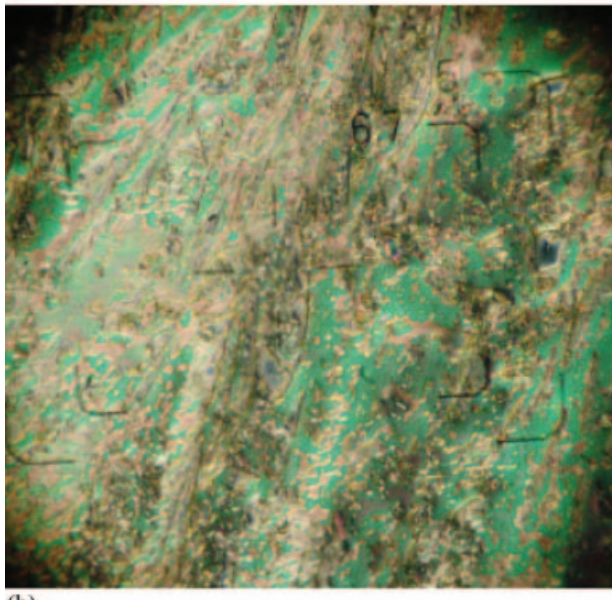

(b)

Figure 3. Photomicrographs of (a) the nematic texture at the clearing point, with round droplets at 282°C, first cooling and (b) the nematic marbled texture at 364°C, first cooling for compound AMF2 (20 x).

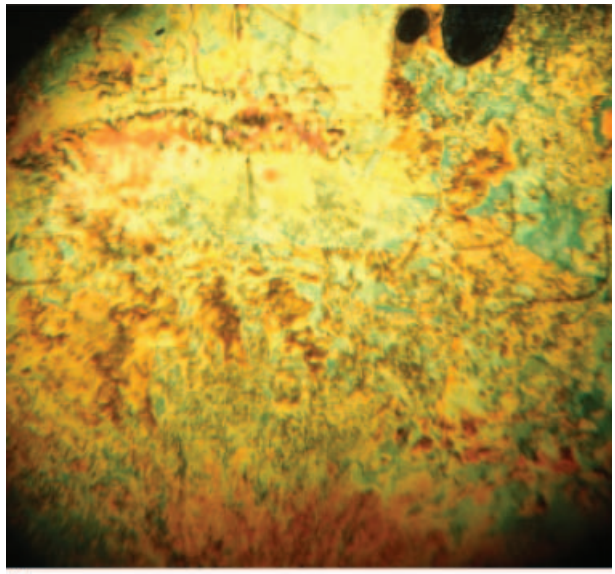

(a)

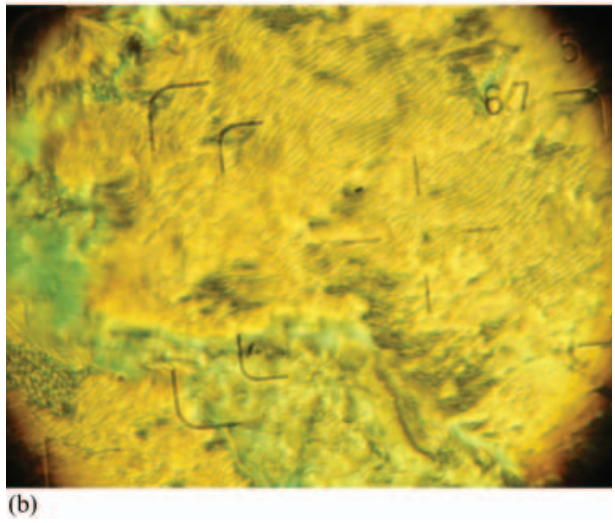

(b)

Figure 4. Photomicrographs of (a) the nematic marbled texture at 175°C, first heating (10 x) and (b) the smectic striated texture at 198°C, first cooling (20 x) for compound AMT2.

which are reported in Table 1 together with the corresponding enthalpy changes. The minor differences can be caused by the different experimental procedures adopted, such as the heating/cooling rate, sample amount, inert (DSC), or oxidative (POM) atmosphere.

The DSC thermograms recorded during a heating–cooling–heating cycle show several transitions for all the azomethine compounds, which confirm the presence of liquid crystalline phases. It is interesting to note that DSC experiments carried out at different scan rates (10 and 90°C min^{-1}) on **AMF1** and **AMT1** samples show different results. In particular, when the adopted scan rates are slow, the cooling curves do not exhibit the transition from the isotropic state to the nematic phase. This is due to the partial thermal decomposition of the materials that occurs at the higher temperatures. The data summarised in Table 1 refer to DSC analyses performed at scan rates of 90°C min^{-1} to avoid the thermal decomposition of the azomethine derivatives. Representative DSC traces of **AMF1** and **AMT2** are shown in Figure 5. Both fluorene-based compounds (**AMF**), which present nematic textures, exhibit two endotherms in the heating scan. The first endothermic peak ascribed to

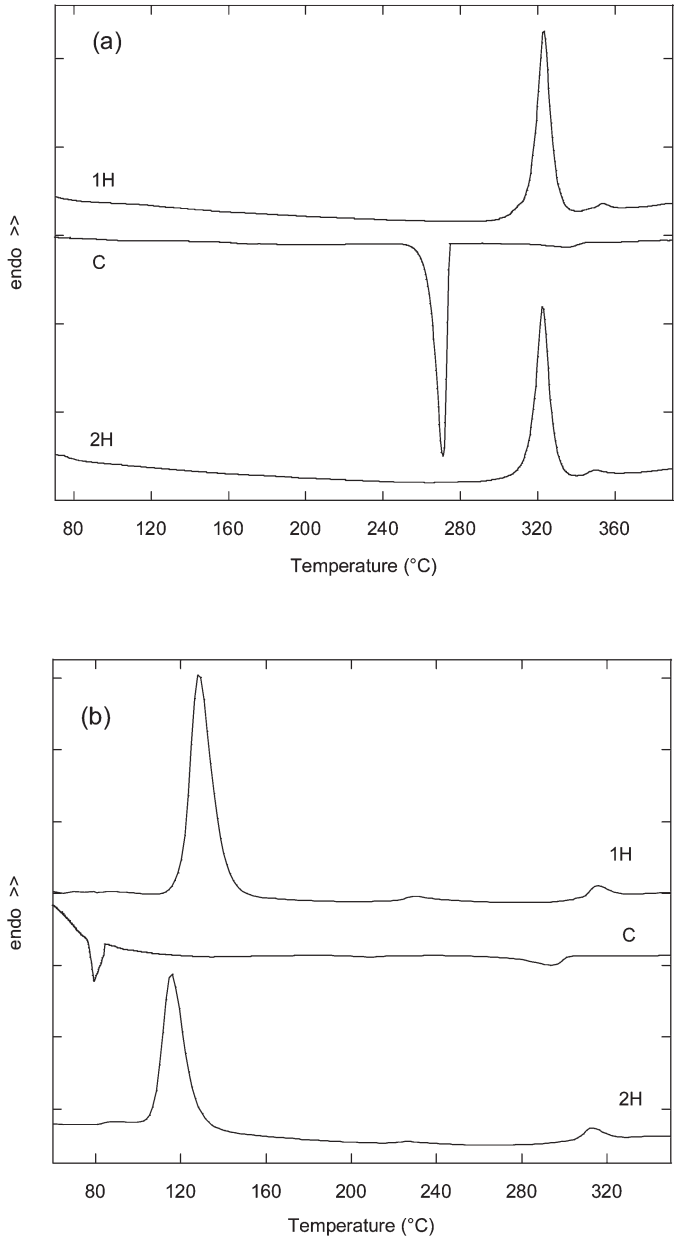

Figure 5. DSC traces of (a) AMF1 and (b) AMT2 recorded at 90°Cmin^{-1}: 1H, heating run of the pristine material; C, successive cooling run; 2H, second heating run.

the crystalline–nematic transition presents a higher enthalpy compared to the other peak due to the nematic–isotropic transition. The subsequent cooling scan shows the same profile as the heating curve, but inverted. Therefore, the reversed phase sequence is produced during the cooling.

Both bithiophene derivatives (**AMT**) show three endothermic peaks in the first heating scan and three exothermic events in the subsequent cooling scan, corresponding to the transitions observed by POM. The enthalpy changes registered by DSC are in agreement with the values usually observed for typical crystalline–smectic, smectic–nematic and nematic–isotropic transitions, confirming the presence of a smectic mesophase and a nematic one (Table 1). Generally, a significant decrease of all the transition temperatures is observed when the lateral methyl substituent is introduced in the backbone. This effect is particularly marked for fluorene-based compounds.

As a general remark, the 3D-LC transition involves most of the energy, again confirming the trend observed in thiophene molecular crystals (*20, 21*).

2.3. X-ray diffraction studies

The nature of the LC phases has been confirmed by X-ray diffraction (XRD) studies. The melt state of the **AMF1** and **AMF2** only showed liquid-like XRD patterns in wide-angle as well as small-angle regions. These mesophases with either Schlieren or marbled textures have been identified as nematic phases (Figure 6(a)). Figure 6(b) shows X-ray diffractograms of **AMT2** at different temperatures. Since **AMT1** and **AMT2** show similar features, only the X-ray diffractogram of the latter is reported as a typical example. At room temperature, the compound displays crystalline XRD patterns, indicating a lamellar structure. When this compound was heated above the first transition temperature determined by DSC, drastic changes in XRD diffractograms occurred. The reflection corresponding to the layer spacing (2.25°, 2θ) shifted to a wider angle (2.51°, 2θ) and its intensity decreased. This behaviour is related to a structural change accompanied by a softening of the alkyl chains, which leads to a change of the positional order in each layer. In addition, wide-angle reflections disappeared completely, revealing that in the mesophase the correlations between adjacent molecules were disrupted. This is indicative of the smectic layer structure, without molecular arrangements within the layers. The layer spacing corresponding to 2.51° is d=3.52 nm, a value slightly smaller than the molecular length evaluated in the most extended conformation using the MATSTUDIO package (L=3.77 nm plus Van der Waals radius, i.e. 4.12 nm) (*22*). This observation constitutes evidence of a molecular tilting typical of the smectic C phase. In spite of the conformational disorder of the hydrocarbon chains, shrinking the long axis, a reliable estimation of tilt-angle can be derived by molecular model calculations using the MATSTUDIO package (*22*), whereby the molecular axis reaches approximately 60°C with respect to the substrate normal. As commonly observed in films of alfa-omega dialkyl-substituted oligomers, cast on polar substrates, the molecules, arranged in a card pack organisation, result in being essentially oriented edge-on with respect to the substrate, so therefore the small spacing (0.4–0.6 nm) typical of the smectic arrangement cannot be detected in Bragg–Brentano geometry.

When the compound is heated above the second transition temperature observed in DSC traces, the reflection in the small-angle region disappears and the X-ray trace only exhibits a broad halo typical of a liquid. This behaviour is related to a structural change accompanied by a loss of positional order, indicating a nematic mesophase.

The presence of a smectic mesophase for the compounds containing thiophene units as compared to the fluorene-containing compounds could be explained by the presence and the position of the aliphatic units, as follows. The methyl groups in the 9-position on fluorene units (**AMF1** and **AMF2**) prevent the close packing of the mesogenic units, hence reducing the reciprocal attraction forces. As a consequence, the self-assembling in a layered structure is suppressed. This fact is usually observed for the fluorene derivatives with alkyl chains in 9-positions, which show only nematic mesophases (*23*). In contrast, the presence of the alkyl units as end-groups in the thiophene derivatives (**AMT1** and

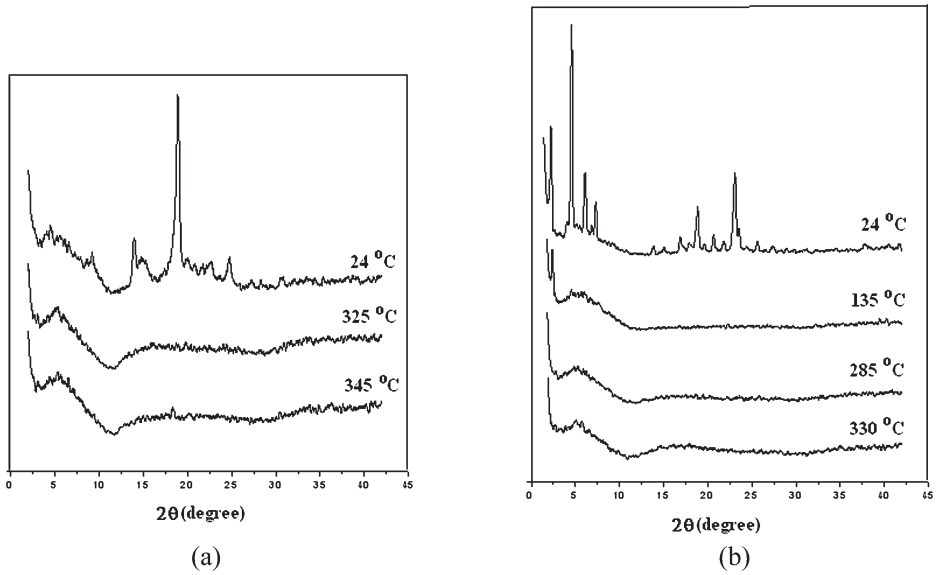

Figure 6. X-ray diffractograms of (a) AMF1 and (b) AMT2 taken at different temperatures.

AMT2) favours the close packing of the mesogenic units. After the crystalline–smectic transition the hexyl end-chains gain enough thermal energy to move, but the layered structure is maintained both due to the strong incompatibility between the aromatic cores and the aliphatic end-groups, and to the strong attractive π-interactions between the aromatic cores. Moreover, the increased chain mobility, and the director tilted with respect to the layer normal and the molecular centres of mass, result in a volume contraction and hence in a layer-spacing decrease, fully in agreement with the XRD investigations.

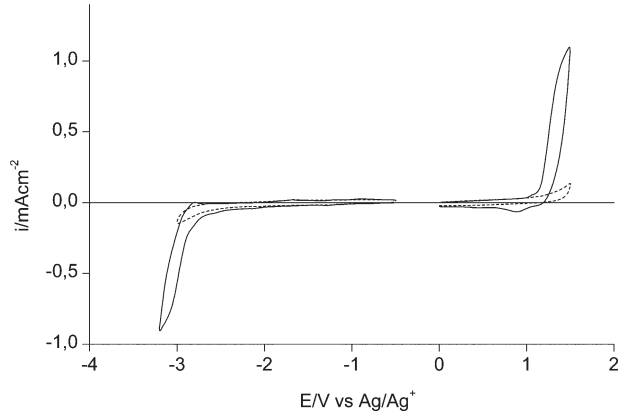

Figure 7. CV curve of AMF1 film.

2.4. *Electrochemistry*

The cyclic voltammogram (CV) of all the films shows irreversible oxidation and reduction processes at the potentials given in Table 2, where highest occupied molecular orbital and lowest unoccupied molecular orbital (HOMO/LUMO) levels, as derived according to (*24*), are reported.

Reduction occurs at about −2.55 V for all azomethines, whereas oxidation occurs at 1.15 V for fluorene derivatives and at 0.9 V and 0.7 V for **AMT1** and **AMT2**, respectively; the higher value for the former is probably due to the more compact crystalline structure. The corresponding electrochemical gaps are comparable with the optical gaps of the films (not reported in the optical characterisation). The CV profile of **AMF1** is reported as an example in Figure 7.

2.5. *Optical properties*

The ultraviolet (UV)-vis absorption and fluorescence spectroscopic data in a dimethylformamide (DMF) solution for all the compounds are summarised in Table 3. A marked broadening of the absorption peak of all the samples can be related to different conformations adopted in the solution. As expected, fluorene derivatives absorb at higher energies as compared to thiophene-based oligomers (see Figure 8). This wavelength red shift (50 nm) of the maximum absorption peak (λ_{max}) for bithiophene derivatives compared to λ_{max} for fluorene derivatives indicated a longer conjugation in the former series, lowering the HOMO–LUMO band gap. The spectra of the methyl containing molecules are blue-shifted with respect to **AMF1** and **AMT1**, due to the enhanced torsion of fluorine–phenyl or thiophene–phenyl bonds in **AMF** and **AMT** classes respectively.

The emission spectra of the **AMF** and **AMT** compounds have been measured by excitation at their absorption wavelength (see Table 3). The red shift observed in the absorption spectra is also evident in the corresponding emission spectra. Bithiophene derivatives (**AMT**) give a larger emission peak wavelength than the fluorene-based molecules (**AMF**) together with a larger Stokes shift (75 nm versus 54 nm for unsubstituted and 91 nm versus 86 nm for methyl-substituted compounds, respectively). This is expected to arise from the presence of a push–pull system (*25*) between the electron-withdrawing group (CH=N) and the electron-donating group (the bithiophene unit). Moreover, a relevant Stokes shift is observed for the compounds containing the methyl group (**AMF2** and **AMT2**) versus the unsubstituted compounds (**AMF1**, **AMT1**). As in the excited state, the quinoidic contribution is larger than in the ground state, the electronic effects (inductive and hyperconjugated) of the methyl group prevail upon the steric effect, accounting for the above observation.

Table 2. Oxidation and reduction potentials (*E*) corresponding HOMO–LUMO levels of the azomethine derivatives.

Code	E_{ox}/V	E_{red}/V	E_{ox}–E_{red}/V[a]	HOMO/eV	LUMO/eV
AMF1	1.12	−2.60	3.72	5.84	2.12
AMF2	1.17	−2.55	3.72	5.89	2.17
AMT1	0.92	−2.60	3.52	5.64	2.12
AMT2	0.69	−2.46	3.15	5.41	2.26

[a]Energy gap measured from electrochemical data according to *E*.

Table 3. Summary of photophysical properties of compounds **AMF** and **AMT**, in DMF solutions.

Compound	$\lambda_{abs.max}$/nm	$\lambda_{em.max}$/nm	Stokes shift/nm	E_g[a]
AMF1	364	418	54	3.40
AMF2	354	440	86	3.50
AMT1	412	488	75	3.00
AMT2	404	495	91	3.06

[a]HOMO–LUMO gap measured according to the maximum of the UV absorption.

The absorption spectra of films spin-coated from the toluene solution are shown in Figure 9. The large blue shift due to the excitonic band is evident in both pristine and annealed (not reported) films, indicating the formation of H-aggregates in all cases (methyl-substituted included). These aggregates heavily quench the luminescence of solid-state samples.

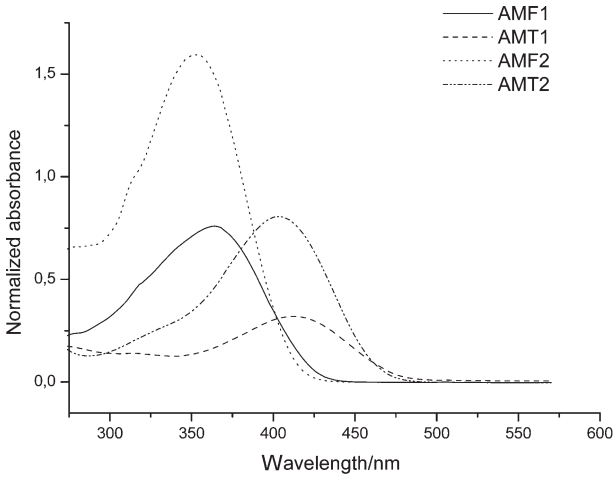

(a)

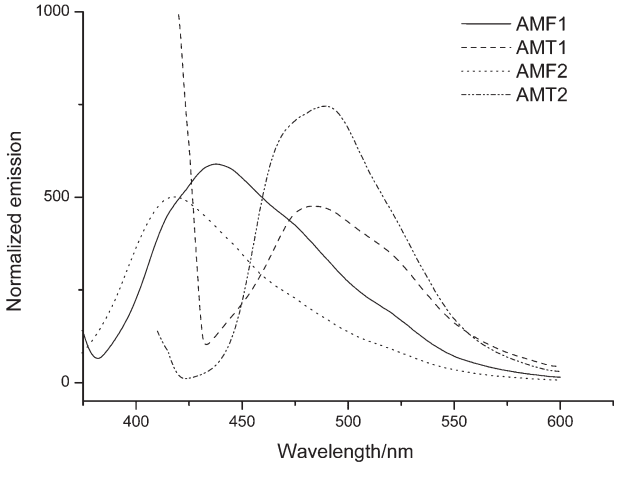

(b)

Figure 8. (a) Absorption and (b) fluorescence spectra of compounds AMT and AMF in DMF solutions.

3. Conclusions

New thermotropic liquid crystalline compounds containing bithiophene or fluorene chromophoric units have been successfully synthesised and characterised. The target compounds present nematic and smectic mesophases with a large mesophase stability. The optical properties have been examined: in solution, blue fluorescence is observed for fluorene-containing compounds and green fluorescence is shown by bithiophene-based derivatives. The introduction of a lateral methyl group on the phenyl rings of the molecules does not prevent H-aggregate formation.

4. Experimental

4.1. Characterisation

^{1}H-NMR spectra were measured with a Bruker Avance instrument (400 MHz). Gas chromatograms (GCs) were performed using an Agilent Network GC System 6890N instrument.

IR spectra were recorded on an FTIR Bruker Vertex 70 Spectrophotometer in transmission mode, by using KBr pellets.

The TGA was carried out by using a Perkin-Elmer TGA-7 apparatus in a nitrogen atmosphere, at a heating rate of $10^{\circ}C\,min^{-1}$.

The melting points, thermal transitions and mesomorphic textures were determined by using an Olympus BH-2 polarised light microscope equipped with a THMS 600/HSF9I heating stage. The optical observations were performed by using clean untreated glass slides.

The DSC measurements were carried out by using a Perkin-Elmer Pyris 1 instrument under a nitrogen atmosphere using heating and cooling rates of 10 and $90^{\circ}C\,min^{-1}$.

Wide angle X-ray diffraction (WAXD) was performed on a Diffractometer Bruker D8 ADVANCE, using the Ni-filtered Cu-Kα radiation (λ=0.1541 nm). A MRI-WRTC-temperature chamber (with nitrogen inert atmosphere) and a MRI-TCPU1-temperature

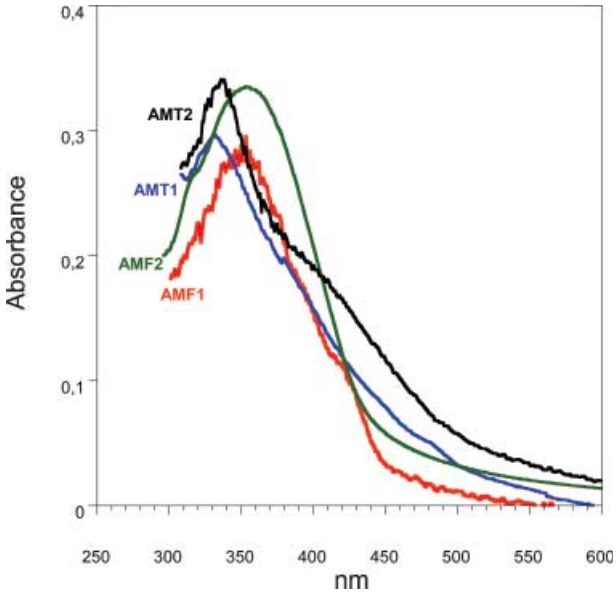

Figure 9. Electronic absorption spectra of spin-coated thin films of the molecules.

control and power unit were used. The working conditions were 36 kV and 30 mA. All the diffractograms were investigated in the range of 1.5° to 40° 2θ, at different temperatures.

Cyclovoltammetric analyses were carried out in acetonitrile (AN) reagent grade (Uvasol, Merck) with a water content of less than 0.01%. The supporting electrolyte tetrabutylammonium perchlorate (Bu_4NClO_4) was previously dried under vacuum at 70°C. Experiments were performed at room temperature under nitrogen in three electrode cells. The counter electrode was platinum and the reference electrode was a silver/0.1 M silver perchlorate in AN (0.34 V *vs.* SCE). The voltammetric apparatus (AMEL, Italy) included a 551 potentiostat modulated by a 568 programmable function generator and coupled to a 731 digital integrator. The working electrode for cyclic voltammetry was a glassy carbon minidisc electrode (0.2 cm^2).

UV-vis absorption and photoluminescence spectra were recorded on a Carl Zeiss Jena SPECORD M42 spectrophotometer and a Perkin-Elmer LS 55 spectrophotometer respectively, in much diluted DMF solutions using 10 mm quartz cells.

4.2. Materials

All the solvents used for the reactions and purifications from Aldrich were used as-received except for the tetrahydrofurane, which was dried by the standard procedure. N-butyllithium in hexane (n-BuLi), 2-isopropoxy-(4,4,5,5-tetramethyl)-1,3,2-dioxoborolane, 2-bromofluorene (95% purity), methyliodide (99% purity), 5-(4,4,5,5-tetramethyl-1,3,2-dioxaborolan-2-yl)-5′-hexyl-2,2′-bithiophene (97% purity), 4-bromobenzaldehyde (99% purity), 4-bromoaniline (97% purity), 4-bromo-3-methyl-aniline (99% purity) and tetrakis(triphenylphosphine)palladium ($(Ph_3P)_4Pd$) were available from Aldrich or Across. Flash chromatography was carried out using silica gel (200–300 mesh ASTM) or LiChroprep RP-18 (Merck). The Suzuki reactions with conventional heating were carried out under nitrogen.

4.3. Synthetic procedures

*4.3.1. (4-Bromobenzylidene)-(4-bromophenyl)-amine (**A1**) and (4-Bromobenzylidene)-(4-bromo-3-methyl-phenyl)-amine (**A2**).*

The preparation of the azomethines **A1** and **A2** was performed by the acid-catalysed condensation reaction of the 4-bromobenzaldehyde (3 mmol, 560 mg) with 4-bromoaniline (3 mmol, 532 mg) and 4-bromo-3-methyl-aniline (3 mmol, 560 mg) respectively, in a 1/1 molar ratio. The synthesis was performed in ethanol (6 ml) under stirring, gently refluxed overnight, using a few drops of glacial acetic acid as catalyst. After cooling, the reaction mixture was kept for 24 h to crystallise a product that was filtered off, washed with water and recrystallised twice from ethanol. Finally the crystals were dried under vacuum for 24 h.

A1: 917 mg product by 98.98% purity determined by GC (retention time (RT): 25.11), yield 91%; m.p. 147°C; ^{1}H-NMR (CD_3Cl, δ: ppm, TMS): 8.38 (s, C<u>H</u>=N), 7.77–7.06 (aromatic H); FTIR ν: cm^{-1} (KBr): 1621 (CH=N stretch), 1581 (C–C ring stretch), 1009 (C–Br stretch).

A2: 889 mg product by 97.18% purity determined by GC (RT: 26.064), yield 84%; m.p. 81°C; ^{1}H-NMR (CD_3Cl, δ: ppm, TMS): 8.4 (s, C<u>H</u>=N), 7.8 –6.75 (aromatic H), 2.3 (s, C<u>H</u>$_3$); FTIR ν: cm^{-1} (KBr): 1620 (CH=N stretch), 1586 (C–C ring stretch), 2872 (C–H bend), 1008 (C–Br).

*4.3.2. 2-(4,4,5,5-Tetramethyl-1,3,2-dioxaborolane-2-yl)-9,9-dimethyl-fluorene (**B2**).*

The product was prepared as reported in (*26*). The identification and the purity of the product were checked by thin layer chromatography and gas chromatography (RT: 21.21).

*4.3.3. Synthesis of 4,4′-bis(5′-n-hexyl-2,2′-bithiophene-5-yl)-benzyliden-aniline (**AMT1**).*

In a Schlenk tube containing 128 mg (0.34 mmol) of 5-hexylbithiophene-2-boronic ester (**B1**), 1.5 ml of dry tetrahydrofuran (THF) and 0.75 ml of a solution of K_2CO_3 [2M] were added, and then the mixture was

stirred for 1 h. Separately, a solution of 57.7 mg (0.17 mmol) of **A1** in 1.5 ml of anhydrous THF was prepared and transferred under nitrogen into the **B1** solution. After the addition of $(Ph_3P)_4Pd$ in catalytic amounts (23 mg), the reaction temperature was increased up to 70°C and the reaction mixture was stirred under reflux overnight with the formation of a precipitate. The reaction was quenched with water and the crude product was filtered and washed several times with diethylether. Then, the product was subjected to purification by recrystallisation from DMF giving 92.4 mg **AMT1** compound in 78% yield. ^{1}H-NMR ($C_2D_2Cl_4$, δ: ppm, TMS): 8.44 (s, C<u>H</u>=N), 7.8–6.6 (aromatic H), 2.8–2.6 (t, C<u>H</u>$_2$–Ar), 1.75–1.55 (m, –CH$_2$–C<u>H</u>$_2$–CH$_3$), 1.4–1.2 (m, –C<u>H</u>$_2$–CH$_2$), 0.95–0.85 (t, –C<u>H</u>$_3$). FTIR ν: cm^{-1} (KBr): 1618 (CH=N stretch), 1601, 1555, 1504 (C–C ring stretch), 3090, 3064 (C–H stretch of the aromatic rings), 2954, 2919, 2851 (C–H stretch of the aliphatic chains), 879, 840, 797 (C–H bend of the aromatic rings), 1445 (absorption band assigned to thiophene ring). Elemental analysis calculated for $C_{41}H_{43}NS_4$ (678.06): C 72.63, H 6.39, N 2.07, S 18.92. Found: C 72.32, H 6.38, N 1.99, S 18.69.

*4.3.4. Synthesis of 4,4′-bis(5′-n-hexyl-2,2′-bithiophene-5-yl)-benzyliden-3-methyl-aniline (**AMT2**).*

Applying the same procedure as described for **AMT1** to 291 mg (0.77 mmol) of **B1**, 136.5 mg (0.39 mmol) of **A2** gave **AMT2** as a brown powder that was recrystallised from an ethyl acetate/dichloromethane mixture at a 1:1 ratio. The final product was obtained as yellow-brownish fine crystals in 83% yield.

^{1}H-NMR ($C_2D_2Cl_4$, δ: ppm, TMS): 8.55 (s, C<u>H</u>=N), 7.9–6.7 (aromatic H), 2.85–2.7 (t, C<u>H</u>$_2$–Ar), 2.52 (s, C<u>H</u>$_3$–Ar), 1.8–1.6 (m, –CH$_2$–C<u>H</u>$_2$–CH$_3$), 1.45–1.22 (m, –C<u>H</u>$_2$–CH$_2$), 0.95–0.85 (t, –C<u>H</u>$_3$). FTIR ν: cm^{-1} (KBr): 1620 (CH=N stretch), 1585, 1554, 1504 (C–C ring stretch), 3092, 3066, 3026 (C–H stretch of the aromatic rings), 2958, 2923, 2853 (C–H stretch of the aliphatic chains), 868, 832, 796 (C–H bend of the aromatic rings), 1448 (absorption band assigned to thiophene ring). Elemental analysis calculated for $C_{42}H_{45}NS_4$ (692.09): C 72.89, H 6.55, N 2.02, S 18.53. Found: C 72.77, H 6.6, N 1.94, S 18.34.

*4.3.5. Synthesis of 4,4′-bis(9,9-dimethyl-fluoren-2-yl)- benzylidene-aniline (**AMF1**).*

In a Schlenk tube, 284.9 mg (0.885 mmol) of **B2**, 150 mg (0.4425 mmol) of **A1** and 61 mg of $(Ph_3P)_4Pd$ were put together. Then, 3 ml of anhydrous THF and 1.5 ml of K_2CO_3 [2M] were added to this mixture under nitrogen. The reaction was stirred at reflux overnight with the formation of a yellow-brownish precipitate, which was isolated by pouring the mixture in cold water followed by a filtration. Later, the crude product was recrystallised from DMF to obtain 196 mg of fine yellow crystals of **AMF1** in 78% yield. ^{1}H-NMR ($C_2D_2Cl_4$, δ: ppm, TMS): 8.6 (s, C<u>H</u>=N), 8.1–7.2 (aromatic H), 1.5 (s, C<u>H</u>$_3$–). FTIR ν: cm^{-1} (KBr): 1621 (CH=N stretch), 1602, 1554, 1514 (C–C ring stretch), 3058, 3030 (C–H stretch of the aromatic rings), 2959, 2922, 2859 (C–H stretch of the methyl groups), 825, 770, 759, 736 (C–H bend of the aromatic rings). Elemental analysis calculated for $C_{43}H_{35}N$ (565.77): C 91.29, H 6.24, N 2.48. Found: C 91.18, H 6.34, N 2.57.

*4.3.6. Synthesis of 4,4′-bis(9,9-dimethyl-fluoren-2-yl)-benzylidene-3′methyl-aniline (**AMF2**).*

Applying the same procedure as described for **AMF1** to 226 mg (0.7 mmol) of **B2**, 123 mg (0.35 mmol) of **A2** and 48 mg $(Ph_3P)_4Pd$ gave a red powder that was recrystallised from ethyl acetate to obtain 148 mg of fine yellow-reddish crystals of **AMF2** in 73% yield.

^{1}H-NMR ($C_2D_2Cl_4$, δ: ppm, TMS): 8.64 (s, C<u>H</u>=N), 8.05–7.2 (aromatic H), 2.45 (C<u>H</u>$_3$–Ar), 1.5 (s, C<u>H</u>$_3$–Fl). FTIR ν: cm^{-1} (KBr): 1624 (CH=N stretch), 1591, 1555, 1515 (C–C ring stretch), 3058, 3034, 315 (C–H stretch of the aromatic rings), 2955, 2920, 2857 (C–H stretch of the methyl groups), 829, 770, 759, 737 (C–H bend of the aromatic rings). Elemental analysis calculated for $C_{44}H_{37}N$ (579.79): C 91.15, H 6.43, N 2.42. Found: C 90.07, H 6.51, N 2.59.

Acknowledgements

We would like to thank Dr. G. Zotti for CV measurements. This work has been partially supported by the European project Research Training Network 'EUROFET', contract no. HPRN-CT-2002-00327 and the Italian project MIUR-FIRB RBNE03S7XZ.

References

(1) Van Breemen J.J.M.; Herwig P.T.; Chlon C.H.T.; Sweelssen J.; Schoo H.F.M.; Setayesh S.; Hardeman W.M.; Martin C.A.; De Leeuw D.M.; Valeton J.J.P.; Bastiaansen C.W.M.; Broer D.J.; Popa-Merticaru A.R.; Meskers S.C.J. *J. Amer. Chem. Soc.* **2006**, *128*, 2336–2345.

(2) Shimizu Y.; Oikawa K.; Nakayama K.; Guillon D. *J. Mater. Chem.* **2007**, *17*, 4223–4229.

(3) Woltman S.J.; Jay G.D.; Crawford G.P. *Nat. Mater.* **2007**, *12*, 929–938.

(4) Seed A. *Chem. Soc. Rev.* **2007**, *36*, 2046–2069 and references therein.

(5) McCulloch I.; Heeney M.; Bailey C.; Genevicius K.; MacDonald I.; Shkunov M.; Sparrowe D.; Tierney S.; Wagner R.; Zhang W.; Chabinyc M.L.; Klim R.J.;

Mc. Gehee M.D.; Toney F.M. *Nat. Mater.* **2006**, *5*, 328–333.
(6) Barbarella G.; Melucci M.; Sotgiu G. *Adv. Mater.* **2005**, *17*, 1581–1593.
(7) O'Neill M.; Kelly S.M. *Adv. Mater.* **2003**, *15*, 1135–1146.
(8) Porzio W.; Destri S.; Giovanella U.; Pasini M.; Marin L.; Iosip M.D.; Campione M. *Thin Solid Films* **2007**, *515*, 7316–7323.
(9) Destri S.; Porzio W.; Marin L.; Damaceanu M.D.; Bruma M. *J. Optoelectr. Adv. Mater.* **2007**, *9*, 1337–1341.
(10) Gray G.W. *Molecular Structure and Properties of Liquid Crystals*; Academic Press: New York, 1962.
(11) Destri S.; Pasini M.; Porzio W.; Zappettini A.; D'Amore F. *J. Opt. Soc. Amer. B.* **2007**, *24*, 1505–1511.
(12) Nalwa H.S., In *Conducting Polymers: Transport, Photophysics and Applications*; Nalwa H.S., Ed., Wiley-Interscience: New York, 1997, Vol. 4, pp. 261–363 and references therein.
(13) Scherf U.; List E.P.J. *Adv. Mater.* **2002**, *14*, 477–487. Redecker M.; Bradley D.D.C.; Inbasekaran M.; Wu W.W.; Woo E.P. *Adv. Mater.* **1999**, *11*, 241–246.
(14) Iwan A.; Sek D. *Progr. Polym. Sci.* **2008**, *33*, 289–345.
(15) Marin L.; Cozan V.; Bruma M. *Rev. Roum. Chim.* **2005**, *50*, 649–653.
(16) Demus D.; Richter L. *Textures of Liquid Crystals*; VEB Deutscher Verlag fur Grundstoffindustrie: Leipzig, 1980.
(17) Baron M. *Pure Appl. Chem.* **2001**, *73*, 845–895.
(18) Serrano J.L.; Romero P.; Marcos M.; Alonso P.J. *J. Chem. Soc., Chem. Commun.* **1990**, *12*, 859–861.
(19) Campoy I.; Marco C.; Gomez M.A.; Fatou J.G. *Polymer Bull.* **1991**, *27*, 81–88.
(20) Destri S.; Mascherpa M.; Porzio W. *Adv. Mater.* **1993**, *5*, 43–45.
(21) Dionigi C.; Stoliar P.; Porzio W.; Destri S.; Cavallini M.; Bilotti I.; Brillante A.; Biscarini F. *Langmuir* **2007**, *23*, 2030–2036 and references therein.
(22) MATSTUDIO modeling release 4.0, Accelrys Inc, 9685 Scranton Rd.n Diego CA (USA), www.accelrys.com, 2006.
(23) Woon K.L.; Aldred M.P.; Vlachos P.; Mehl G.H.; Stirner T.; Kelly S.M.; O'Neill M. *Chem. Mater.* **2006**, *18*, 2311–2317.
(24) Janietz S.; Bradley D.D.C.; Grell M.; Giebeler M.; Inbasekaran M.; Woo E.P. *Appl. Phys. Lett.* **1998**, *73*, 2453–2455.
(25) Hohnholz D.; Schweikart K.-H.; Subramanian L.R.; Wedel A.; Wischert W.; Hanack M. *Synth. Met.* **2000**, *110*, 141–152.
(26) Destri S.; Pasini M.; Porzio W.; Gigli G.; Pisignano D.; Capolupo C. *Synth. Met.* **2003**, *138*, 289–293.